One- and Two-Dimensional Electron Spin Echo Envelope Modulation Study of the Intermediate Electron Acceptor Pheophytin in ^{14}N- and ^{15}N-Labeled Photosystem II

Yiannis Deligiannakis* and A. William Rutherford

Contribution from the Section de Bioénergétique (URA CNRS 2096), Département de Biologie Cellulaire et Moléculaire, CEA Saclay, 91191 Gif-sur-Yvette, France

Received September 19, 1996[⊗]

Abstract: The intermediate electron acceptor of the photosystem II (PSII) reaction center, which is a pheophytin-α (Pheo) molecule, was studied by pulsed EPR. Electron spin echo envelope modulation (ESEEM) experiments were carried out in ^{14}N- and ^{15}N-labeled PSII reaction centers. The assignment of the ESEEM frequencies was achieved by the application of three-pulse (stimulated echo) and four-pulse 2D-HYSCORE sequences. Computer simulations of the ^{14}N- and ^{15}N-stimulated ESEEM spectra were performed, yielding a complete set of hyperfine and quadrupole coupling constants of the four nitrogens of the macrocycle of the pheophytin. The nitrogen hyperfine couplings are characterized by considerable anisotropy while the isotropic part is either smaller or much larger than the nuclear Larmor frequency. The present results show that the spin density distribution on the $Pheo^-$ in PSII is highly asymmetric. In agreement with earlier theoretical predictions for $Pheo^-$ *in vitro*, the ESEEM data show that in PSII the two unprotonated nitrogens bear considerable spin density while the protonated nitrogens bear a small fraction of the spin density.

Introduction

In photosynthesis, reaction centers mediate the light-induced charge separation and subsequent conversion of light into chemical energy. In the photosystem II (PSII) reaction center a plastoquinone-9 (Q_A) and a pheophytin-α (Pheo) molecule mediate the photoinduced electron transfer from the primary donor, P_{680}, to a plastoquinone pool.[1ab] The pheophytin molecule forms part of the primary radical pair $[P^+_{680}Pheo^-]$[1] and thus plays a key role in the photoinduced electron transport in PSII. Its spatial proximity to the Q_A and the non-heme iron, Fe^{2+}($S = 2$), of the acceptor side in the PSII reaction center is evidenced from the EPR spectrum of the $Pheo^-Q_A{}^-Fe^{2+}$ ($S = 2$) state.[2] In a recent study we showed that the non-heme iron acts as a moderate relaxation enhancer of the $Pheo^-$, and from the observed relaxation enhancement the distance between the pheophytin and the non-heme iron is estimated to be 20 ± 4.2 Å.[3]

An understanding of the electron transfer dynamics from first principles requires the knowledge of the spatial and the electronic structure of the donor and acceptor molecules. The detailed electronic structure information required for this analysis can be obtained by using electron paramagnetic resonance techniques like electron spin echo envelope modulation (ESEEM)[4ab] and electron nuclear double resonance (ENDOR).[4c] The $Pheo^-$ radical *in vitro* has been studied by ^1H-ENDOR[5abd] and ^{14}N-ENDOR in solution;[5c] for a review see ref 5e. A more recent ^1H-ENDOR study of the Pheo anion radical *in vitro* as well as in PSII membranes and D_1D_2cyt b_{559} particles[5d] revealed differences between the spin-density distributions on the Pheo *in vitro* and in the reaction center of PSII.

The ESEEM technique is eminently suited for measuring low nuclear spin resonance frequencies.[4a,b] Its application for the study of chlorophyll radicals, photosynthetic paramagnetic centers in bacterial photosynthetic systems,[6] the primary donor of photosystem I,[7] and in a number of paramagnetic centers in photosystem II[8] has been fruitful. Furthermore, in complex biological systems with multiple nuclei coupled to the same

[⊗] Abstract published in *Advance ACS Abstracts*, April 15, 1997.

(1) (a) Hansson, Ö.; Wydrzynski, T. *Photosynth. Res.* **1990,** 23, 131. (b) Renger, G. In *Topics in Photosynthesis*; Barber, J., Ed.; Elsevier: Amsterdam, 1992; Vol. 11, p 25. (c) Shuvalov, V. A.; Klimov, V. V.; Dolan; E.; Parson; W. W.; Ke; B. *FEBS Lett.* **1980,** 118, 279.

(2) (a) Klimov. V. V.; Dolan. E.; Shaw, E. R.; Ke, B. *Proc. Natl. Acad. Sci. U.S.A.* **1980,** 77, 7227. (b) Rutherford, A. W.; Zimmermann, J. L. *Biochim. Biophys. Acta* **1984,** 767, 168.

(3) Deligiannakis, Y.; Rutherford, A. W. *Biochemistry* **1996**, *35*, 11239.

(4) (a) Kevan, L.; Bowman, M. K. *Modern Pulsed and Continuous Wave Electron Spin Resonance*; John Wiley & Sons: New York, 1990. (b) Dikanov, S. A.; Tsvetkov, Y. D. *ESEEM spectroscopy;* CRC Press: Boca Raton, FL, 1992. (c) Kevan, L; Kispert, L. D. *Electron Spin Double Resonance Spectroscopy*; Wiley & Sons: New York, 1976. (d) Dikanov, S. A.; Yudanov, V. F.; Tsvetkov Yu., D. *J. Magn. Reson.* **1979**, *34*, 631.

(5) (a) Fujita, I.; Davis, M. S.; Fajer. *J. Am. Chem. Soc.* **1978**, 100, 6280. (b) Fajer, J.; Davis, M. S.; Forman, A.; Klimov, V. V.; Dolan, E.; Ke, B. *J. Am. Chem. Soc.* **1980**, 102, 7143. (c) Lendzian, F.; Mobius, K.; Lubitz, W. *Chem. Phys. Lett.* **1982,** 90, 375. (d) Lubitz, W.; Isaakson, R. A.; Okamura, M. Y.; Abresch, E. C.; Plato, M.; Feher, G. *Biochim. Biophys. Acta* **1989** 977, 227. (e) Lubitz, W. In *Chlorophylls, CRC Handbook*; Scheer, H., Ed.; CRC Press: Boca Raton, FL, 1991; pp 903−944.

(6) (a) De Groot, A.; Hoff, A. J.; De Beer, R.; Scheer, H. *Chem. Phys. Lett*. **1985**, *113*, 286. (b) Hoff, A. J.; De Groot, A.; Dikanov, S. A.; Astashkin, A. V.; Tsvetkov, Y. D. *Chem. Phys. Lett.* **1985**, *118*, 40. (c) Lin, C. P.; Bowman, M. K.; Norris, J. R. *J. Chem. Phys.* **1985**, *85*, 56. (d) Astashkin, A. V.; Dikanov, S. A.; Tsvetkov, Y. D. *Chem. Phys. Lett.* **1986**, *130*, 337. (e) Astaskin, A. V.; Dikanov, S. A.; Tsvetkov, Y. D. *Chem. Phys. Lett*. **1988**, *152*, 258. (f) Käss, H.; Rautter, J.; Bönigk, B.; Höfer, P.; Lubitz, W. *J. Phys. Chem.* **1995**, *99*, 436. (g) Bosch, M. K.; Gast, P.; Hoff, A. J.; Spoalov, A. P.; Tsvetkov, Y. D. *Chem. Phys. Lett.* **1995**, *239*, 306.

(7) (a) Bowman, M. K.; Norris, J. R.; Thurnauer, M. C.; Warden, S. A.; Dikanov, S. A.; Tsvetkov, Y. D. *Chem. Phys. Lett.* **1978**, *55*, 570. (b) Astashkin, S. V.; Dikanov, S. A.; Tsvetkov, Y. D.; Goldfeld, M. G. *Chem. Phys. Lett.* **1987**, *134*, 438. Davis, I. H.; Heathcote, P.; MacLachlan, D. J.; Evans, M. C. W. *Biochim. Biophys. Acta* **1993**, *1143*, 183. (c) Käss, H.; Bittersmann-Weidlich, E.; Andréasson, L.-E.; Bönigk, B.; Lubitz, W. *Chem. Phys.* **1995**, *194*, 419. (d) Käss, H.; Fromme, P.; Lubitz, W. *Chem. Phys. Lett*. **1996**, *257*, 197.

(8) (a) Evelo, R. G.; Dikanov, S. A.; Hoff, A. J. *Chem. Phys. Lett.* **1989**, *157*, 25. (b) Evelo, R. G.; Hoff, A. J.; Dikanov, S. A.; Tyryshkin, A. M. *Chem. Phys. Lett.* **1989**, *161*, 479. (c) Britt, R. D.; Zimmermann, J.-L.; Sauer, K.; Klein, M. P. *J. Am. Chem. Soc*. **1989** *114*, 3715. (d) De Rose, V. J.; Yachandra, V. K.; McDermott, A. E.; Britt, R. D.; Sauer, K.; Klein, M. P. *Biochemistry* **1991**, *30*, 1335. (e) Zimmerman, J.-L.; Boussac, A.; Rutherford, A. W. *Biochemistry* **1993**, *32*, 4831. (f) Tang, X.-S.; Diner, B. A.; Larsen, B. S.; Gilchrist, M. L.; Lorigan. G. A.; Britt, R. D. *Proc. Nat. Acad. Sci. U.S.A.* **1994**, *91*, 704. (g) Astashkin, A. V.; Kawamori, A.; Kodera, Y.; Kuroiwa, S.; Akabori, K. *J. Chem. Phys*. **1995**, *102*, 5583. (h) Deligiannakis, Y.; Boussac, A.; Rutherford, A. W. *Biochemistry* **1995**, *34*, 16030.

S0002-7863(96)03293-3 CCC: $14.00

electron spin, two-dimensional hyperfine sublevel correlation spectroscopy (HYSCORE)[9] is a promising method for elucidating the hyperfine couplings.[6f,9]

In the literature there is no ESEEM study of a Pheo molecule in either *in vitro* or *in vivo* systems. In the present work we report an ESEEM study of the Pheo anion in the PSII reaction center. In contrast to ENDOR spectroscopy the present ESEEM measurements can afford, in addition to the anisotropic hyperfine coupling constants, the nuclear quadrupole interaction parameters. The hyperfine and quadrupole tensors for the four nitrogens of the Pheo macrocycle are assigned by numerical simulations and 2D-HYSCORE experiments in [^{14}N]- and [^{15}N]-PSII reaction centers.

Experimental Section

Sample Preparation. PSII membranes were isolated from market spinach as described previously[12a] with the modifications described by Boussac and Rutherford.[12b] ^{15}N-labeled membranes were prepared from spinach grown in a medium supplemented with ^{15}N-labeled minerals (98% $K^{15}NO_3$, $(^{15}NH_4)_2SO_4$, $Ca(^{15}NO_3)$, Eurisotop, Saclay, France). Tris treatment to remove the Mn cluster[12c] was performed by incubating these PSII membranes (0.5 mg of chlorophyll/mL) in 0.8 M Tris−HCL (pH 8.3) and 5 mM NaEDTA for 30 min at 0 °C under room light. The Tris-treated membranes were pelleted and washed once in a buffer containing 60 mM HEPES (pH 8.0), 10 mM NaCl, and 5 mM $MgCl_2$ and resuspended in the same buffer at 5 mg of chlorophyll/mL final concentration. The Pheo$^-$ radical was induced by a procedure which involved incubation of the membranes under reducing conditions ($E_h = -430 \pm 20$ mV) for 60 min at 5 °C in the dark followed by illumination at 15 °C for 12 min.[3] No redox mediator was used. The redox potential was adjusted by sodium dithionite under anaerobic conditions and was measured in the sample with a platinum electrode and with a calomel reference electrode (Russell pH, Auchtermuchty, U.K.) connected to a Tacussel pH/millivolt meter (Tacussel, Villeurbanne, France). Measured redox potentials were normalized to the standard hydrogen electrode, calibrating the electrode using saturated quinhydrone (potential 286 mV, at pH 6.5).

Spectroscopic Measurements. Continuous-wave (cw) EPR spectra were recorded at liquid helium temperatures with a Bruker ER 200D X-band spectrometer equipped with an Oxford Instruments cryostat. The microwave frequency and the magnetic field were measured with a microwave frequency counter, HP 5350B, and a Bruker ER035M NMR gaussmeter, respectively.

Pulsed EPR was performed with a Bruker ESP 380 spectrometer with a dielectric resonator described previously;[8h] typical instrument deadtime was 100 ns. The field swept spectra were obtained by recording the amplitude of the echo as a function of the magnetic field after a two-pulse sequence ($\pi/2-144$ ns$-\pi$); the durations of the $\pi/2$ and π pulses were 32 and 64 ns, respectively. In the three-pulse ($\pi/2-\tau-\pi/2-T-\pi/2$) ESEEM data the amplitude of the stimulated echo as a function of $\tau + T$ was measured at a frequency near 9.6 GHz at a magnetic field corresponding to the maximum intensity of the field swept spectrum. The minimum interpulse T was 16 ns and was incremented in steps of 8 ns; the duration of the $\pi/2$ pulse was 16 ns, corresponding to $\mathbf{B}_1 \approx 6$ G. Measurements were carried out at 40 K with a repetition rate of 10 Hz and τ values from 120 to 720 ns. 2D-HYSCORE spectra were recorded using the sequence $\pi/2-\tau-\pi/2-t_1-\pi-t_2-\pi/2-\tau-$echo, where the echo is measured as a function of t_1 and t_2.[9a] The durations of the $\pi/2$ and π pulses were 16 and 32 ns, respectively, with equal amplitudes. A total of 170−256 points were recorded in each dimension for a series of τ values from 80 to 368 ns, while t_1 and t_2 were incremented in steps of 32 ns from their initial values. To remove the unwanted echoes, the appropriate phase-cycling procedures in the stimulated echo[13] and HYSCORE[14] experiments were applied.

Data Manipulation. (i) 1D-Stimulated Echo ESEEM. Deadtime reconstruction was performed according to Mims.[15] Prior to Fourier transform the time-domain echo decay was factored out by subtraction of a linear function, and zero-filling to 512 points was performed followed by a tapering with a Hamming window.

(ii) 2D HYSCORE ESEEM. The background decay in both t_1 and t_2 dimensions was subtracted using a linear function followed by zero-filling to 512 points in two dimensions and tapering with a Hamming window; then Fourier transform was carried out in both dimensions. The spectra shown are in the absolute value mode.

Simulation of the ESEEM Spectra. ^{14}N ($S = 1/2$, $I = 1$). The spin Hamiltonian for an $S = 1/2$, $I = 1$ system characterized by an isotropic **g** tensor with magnetic field $\mathbf{B}_0$ along z is[4b]

$$H = \mathbf{g}\mu_B\mathbf{B}_0S_z - \mathbf{g}_N\mu_N\mathbf{B}_0I_z + \mathbf{S}\cdot\mathbf{A}\cdot\mathbf{I} + \mathbf{I}\cdot\mathbf{Q}\cdot\mathbf{I} \quad (1)$$

where the hyperfine coupling tensor **A** has principal values (A_{xx}, A_{yy}, A_{zz}) and consists of the isotropic contribution A_{iso} and the traceless tensor **T** describing the anisotropic hyperfine coupling. The nuclear quadrupole interaction, **Q**, is traceless by definition. In its principal axis system the final term in eq 1 is expressed in the form

$$\mathbf{I}\cdot\mathbf{Q}\cdot\mathbf{I} = K[3I_z^2 - I^2 + \eta(I_x^2 - I_y^2)] \quad (2)$$

where K represents the quadrupole coupling constant $e^2qQ/4h$ and η is the asymmetry parameter of the electric field gradient. The energies and eigenfunctions are calculated numerically for each spin manifold, and the three-pulse modulations were calculated with the relations derived by Mims.[17] Numerical simulations of the ^{14}N-ESEEM spectra were performed with a FORTRAN program generously provided by J. McCracken.

^{15}N ($S = 1/2$, $I = 1/2$). The stimulated echo modulation amplitude $E(\tau,T)$ of a single $I = 1/2$ nucleus coupled to an electron spin $S = 1/2$ is given by[4b]

$$E(\tau,T) = 1 - k[\sin^2(\pi\nu_\alpha\tau)\sin^2(\pi\nu_\beta(\tau+T)) + \sin^2(\pi\nu_\beta\tau)\sin^2(\pi\nu_\alpha(\tau+T))] \quad (3)$$

The fundamental hyperfine frequencies for the two electron spin manifolds are

$$\nu_{\alpha(\beta)} = [(A/2m\nu_I)^2 + (B/2)^2]^{1/2} \quad (4a)$$

where, for an axial nuclear hyperfine coupling ($A_{iso} - T$, $A_{iso} - T$, $A_{iso} + 2T$)

$$A = A_{iso} + T(3\cos^2\theta - 1) \quad (4b)$$

$$B = 3T\cos\theta\sin\theta \quad (4c)$$

In the above relations ν_I is the nuclear Larmor frequency, A_{iso} the isotropic hyperfine coupling, and θ the angle describing the direction of the laboratory magnetic field with respect to the principal axis of the hyperfine tensor. In the case of several nuclei coupled to the same

(9) (a) Höffer, P., Grupp, A.; Nedenführ, H.; Mehring, M. *Chem. Phys. Lett.* **1986**, *132*, 279. (b) Shane, J. J.; Höfer, P.; Reijerse, E. J.; De Boer, E. J. *J. Magn. Reson.* **1992,** 99, 596. (c) Höffer, P. In *Electron Magnetic Resonance of Disordered Systems EMARDIS-91*; Yudanov, N., Ed.; World Scientific: Singapore, 1991; p 1. (d) Höffer, P. *J. Magn. Reson., Ser. A* **1994**, *111*, 77. (e) Shane, J. J.; van der Heijden, P. A. A. W.; Reijerse, E. J.; de Boer, E. *Appl. Magn. Reson.* **1994**, *6*, 427. (f) Shane, J. J. Doctoral Thesis, University of Nijmegen, 1993.

(10) (a) Dikanov, S. A.; Samoilova, R. I.; Smieja, J. A.; Bowman, M. K. *J. Am. Chem. Soc.* **1995,** *117*, 10579. (b) Kofman, V.; Shane, J. J.; Dikanov, S. A.; Bowman, M. K.; Libman, J.; Shanzer, A.; Goldfarb, D. *J. Am. Chem. Soc.* **1995**, *117*, 12771. (c) Shergill, J. K.; Joannou, C. L.; Mason, J. R.; Cammack, R. *Biochemistry*, **1995**, *34*, 16533. (d) Kofman, V.; Farver, O.; Pecht, I.; Goldfarb, D. *J. Am. Chem. Soc.* **1996**, *118*, 1201.

(11) (a) Riejerse, E. J.; Dikanov, S. A. *Pure Appl. Chem.* **1992**, *68*, 789. (b) Dikanov, S. A.; Bowman, M. K. *J. Magn. Reson., A* **1995**, *116*, 125.

(12) (a) Berthold, D. A.; Babcock, G. T.; Yocum, C. F. *FEBS Lett.* **1981,** *134*, 231. (b) Boussac, A.; Rutherford, A. W. *Biochemistry* **1988**, *27*, 3476. (c) Yocum, C., Yerkes, C. T.; Blankenship, R. E.; Sharp, R; R.; Babcock, G. T. *Proc. Natl. Acad. Sci. U.S.A.* **1981**, *78*, 7507.

(13) Fauth, J. M.; Schweiger, A.; Braunschweiler, L.; Forrer, J.; Ernst, R. *J. Magn. Reson.* **1986,** *66*, 64.

(14) Gemperle, G., Aebli, G.; Schweiger, A., Ernst, R. R. *J. Magn. Reson.* **1990**, *88*, 241.

(15) Mims, W. B. *J. Magn. Reson.* **1984,** *59*, 291.

(16) Van Mieghem, F. J. E.; Nitschke, W.; Mathis, P.; Rutherford, A. W. *Biochim. Biophys. Acta* **1989**, *977*, 207.

(17) (a) Mims, W. B. *Phys. Rev. B5* **1972**, 2409. (b) Mims, W. B. *Phys. Rev. B6* **1972**, 3543.

electron spin, the resulting modulation functions for each spin manifold were multiplied in the time domain[4d] according to

$$E(\tau,T) = (1/2)(\prod_i E_\alpha(\tau,T) + \prod_i E_\beta(\tau,T)) \quad (5)$$

In orientationally disordered systems, the line shapes for the basic ESEEM frequencies ν_α and ν_β are determined by the angular dependence of the line positions according to eq 4, the modulation depth factor, which is usually written in the form $k = (\nu_I B/\nu_\alpha\nu_\beta)^2$ and the statistical weight factor (1/2) sin θ dθ. The powder average in the time domain is calculated as

$$E(\tau,T)_{\text{powder}} = (1/4\pi)\int_{\phi=0}^{2\pi}\int_{\theta=0}^{\pi} E(\tau,T,\theta,\phi)\sin\theta\, d\theta\, d\phi \quad (6)$$

2D-ESEEM. In the 2D-HYSCORE experiment the nuclear spin transitions in the two M_s manifolds are correlated to each other by cross-peaks in the 2D-frequency domain.[9]

In the case of an anisotropic hyperfine interaction the correlation peaks of a powder 2D spectrum become ridges.[9c,d,11] In the case of $S = 1/2$, $I = 1/2$ the contour line forms of the correlation ridges can be calculated from the relations[11b]

$$\nu_{\alpha(\beta)} = [Q_{\alpha(\beta)}\nu_{\alpha(\beta)}{}^2 + G_{\alpha(\beta)}{}^2]^{1/2} \quad (7)$$

where

$$Q_{\alpha(\beta)} = (2A_{\text{iso}} + 4\nu_I + T)/(2A_{iso} \pm 4\nu_I + T)$$

and

$$G_{\alpha(\beta)} = \pm 2\nu_I(4\nu_I{}^2 - A_{\text{iso}}{}^2 + 2T^2 - TA_{\text{iso}})/(2A_{\text{iso}} + T \pm 4\nu_I)$$

These relations do not depend on the time τ between the first and the second pulses and thus correspond to ideal "suppression free" 2D spectra.[11b] Also, since no information about the relative phase of the nuclear transitions is contained in these relations, only the shape of the ridges can be calculated. The amplitude coefficients of the cross-peaks in the 2D-HYSCORE spectrum are given by the relation

$$c^2(s^2) = |(\nu_I{}^2 - (1/4)(\nu_\alpha \pm \nu_\beta)^2)/\nu_\beta\nu_\alpha| \quad (8)$$

and they determine the sign of the phase modulation:[9,11] In the limit of weak hyperfine interaction, the contributions with positive phase modulation (which have an amplitude coefficient c^2) dominate; consequently in the frequency domain the cross-peaks are predominantly in the (+, +) quadrant.[9,11] In the limit of strong hyperfine interaction, the contributions with negative phase modulation (which have an amplitude coefficient s^2) dominate; in this case the cross-peaks are predominantly in the (+, −) quadrant. When the hyperfine and Zeeman couplings have similar magnitude, then the cross-peaks in the 2D-HYSCORE spectrum have comparable intensity in both quadrants.

To obtain a more basic understanding of the utility of the 2D technique, we have calculated a series of suppression free 2D spectra for characteristic sets of hyperfine couplings by using eq 7. Representative correlation ridges calculated in this way are displayed in Figure 5; in each panel in this figure only the quadrant with the stronger lines is displayed. In the case of an $I = 1/2$ nucleus coupled to an $S = 1/2$ electron spin with small anisotropic hyperfine interaction, the correlated peaks in the frequency-domain 2D spectrum appear in the (+, +) or in the (+, −) quadrant in the case of $|A_{\text{iso}}| < 2\nu_I$ (see for example Figure 5A) or $|A_{\text{iso}}| > 2\nu_I$ (see for example Figure 5E), respectively.[9] The anisotropy of the hyperfine interaction is manifested as arc-shaped cross-peaks in the 2D spectrum.[9d,11] In the case when the anisotropic hyperfine interaction becomes the same order as the isotropic hyperfine interaction, the ridges are more extended, and in the case when $|A_{\text{iso}}| < 2\nu_I$, the arcs cross the diagonal; see Figure 5B. In the ideal case of fully resolved ridges, the principal values of the hyperfine interaction tensor may be estimated from the 2D spectrum.[9d,11b] In the "matching" condition[18] when $|2A_{\text{iso}} + T| = 4\nu_I$, the ridges become almost parallel to the frequency axes, see Figure 5C, and according to eq 8 they have comparable intensities in both the (+, +) and the (+, −) quadrants.[11]

Computer simulations of ^{15}N- and ^{14}N-ESEEM spectra obtained in this study were undertaken to determine the hyperfine and quadrupole interaction constants. The procedure was the following: a set of hyperfine coupling constants was determined from the HYSCORE experiment and the numerical simulations of the stimulated ESEEM of the Pheo⁻ in [^{15}N]PSII. The ^{14}N hyperfine coupling values were scaled from those determined for ^{15}N nuclei; the nuclear quadrupole parameter e^2qQ/h, the asymmetry parameter η, and the three Euler angles[20b] α, β, and γ, which concern the relative orientation between the tensors **A** and **Q**, were evaluated by the fitting of simulations to the experimental spectra. For the simulation of the observed spectra, the requirements were to reproduce the spectral peak positions, the modulation amplitude as a percentage of the maximum recorded echo amplitude, and the τ suppression behavior.[17] ESEEM simulations where the above criteria were satisfied could only be obtained for hyperfine couplings with comparable anisotropic and isotropic parts. Since nonideal pulses or partial excitation are not taken into account in our simulations, the relative intensities could not be reproduced exactly.[30] In general, the errors associated with the various coupling parameters are on the order of 10%.

Results

The pheophytin anion radical, Pheo⁻, was trapped after illumination of the PSII membranes under strongly reducing conditions as in ref 3. The echo-detected EPR spectrum of Pheo⁻ recorded in Mn-depleted [^{14}N]PSII membranes is displayed in Figure 1C[20c]; the corresponding cw EPR spectrum, displayed in Figure 1B, consists of a structureless derivative with $\Delta H_{\text{pp}} = 12.5 \pm 0.5$ G and $\mathbf{g} = 2.0033$, i.e., the EPR characteristics of Pheo⁻.[2a,3] Under these conditions the primary quinone is double reduced and probably protonated[16] while all the stable cationic paramagnetic centers of PSII[1a] (the stable tyrosine Y_D, the Cyt b_{559}) are reduced. No other signals are detected in the 3−5 kG magnetic field range.

Stimulated Echo ESEEM of Pheo⁻ in [^{14}N]PSII. In Figure 2A the stimulated echo decay is displayed. In order to avoid missing modulation frequencies due to τ suppression effects,[17] the echo decay was recorded at several τ values. The traces are dominated by a modulation component with a period of

(18) (a) Lai, A.; Flanagan, H. L.; Singel, D. J. *J. Chem. Phys.* **1988,** *89*, 7161. (b) Reijerse, E. J.; Dikanov, S. A. *J. Chem. Phys.* **1991**, *95*, 836. (c) Larsen, R. G.; Halkides, C. J.; Singel, D. J. *J. Chem. Phys.* **1993**, *98*, 6705. (d) Gerfen, G. J.; Singel, D. J. *J. Chem. Phys.* **1994**, *100*, 1994.

(19) (a) Dikanov, S. A.; Tsvetkov, Y. D.; Bowman, M. K.; Astashkin, A. V. *Chem. Phys. Lett.* **1982**, *90*, 149. (b) Mims, W. B.; Peisach, J. *J. Chem. Phys.* **1978**, *69*, 4921. (c) Flanagan, H. L.; Singel, D. J. *J. Chem. Phys.* **1987**, *87*, 5606. (d) Reijerse, E. J.; Keijzers, C. P. *J. Magn. Reson.* **1987**, *71*, 83.

(20) (a) In the case of "exact cancellation", the ESEEM spectrum contains three sharp low-frequency lines, with maxima at frequencies given by the relations $\nu_+ = 3K(1 + \eta)$, $\nu_- = 3K(1 - \eta)$, and $\nu_0 = 2K\eta$, and a double-quantum ($\Delta m_I = 2$) line has maximum intensity at a frequency which is approximated by $\nu_{\text{dq}} \approx 2[(\nu_I + A/2)^2 + K^2(3 + \eta^2)]^{1/2}$. (b) Different conventions are sometimes used for the Euler angles. We use the convention of Mathews, J.; Walkers, R. L. *Mathematical Methods of Physics*; W. A. Benjamin, Inc.: New York, 1970; p 404. I.e., α is a positive rotation about the z axis, β is a positve rotation about the Y' axis, and γ is a positive rotation about the z' axis. (c) In systems with large **g** anisotropy and deep modulation, the field swept electron spin echo detected spectrum may differ considerably from the absorption EPR spectrum due the selectivity of the pulses, nuclear modulation, and τ-supression effects (see: Golfarb, D.; Kevan, L. *J. Magn. Reson.* **1988**, 76, 276; see also ref 4a). In the present case, i.e., a narrow spectrum with almost isotropic g, this effect is small; furthermore, due to the nonselective excitation and detection used, the echo detected spectrum is ∼0.4 G broader than the cw EPR spectrum and no other line shape distortion is detectable. (d) The cw spectrum could be simulated using any of the sets of nitrogen hyperfine tensors in Table 1 in combination with the proton hyperfine tensors from the ENDOR study in ref 5d. It is of note that the line width is determined by the large isotropic methyl protons rather than by the nitrogen couplings. (e) Note added during revision: The prediction that the spin density on the nitrogens of the pheophytin-α anion are likely to be insensitive to the environment seems to be borne out by the recent ESEEM experiments on the pheophytin-α anion in pyridine. These preliminary experiments show ^{14}N couplings which are very similar to those reported here for Pheo⁻ in PSII (Y.D., A.W.R., and F. MacMillan, unpublished work).

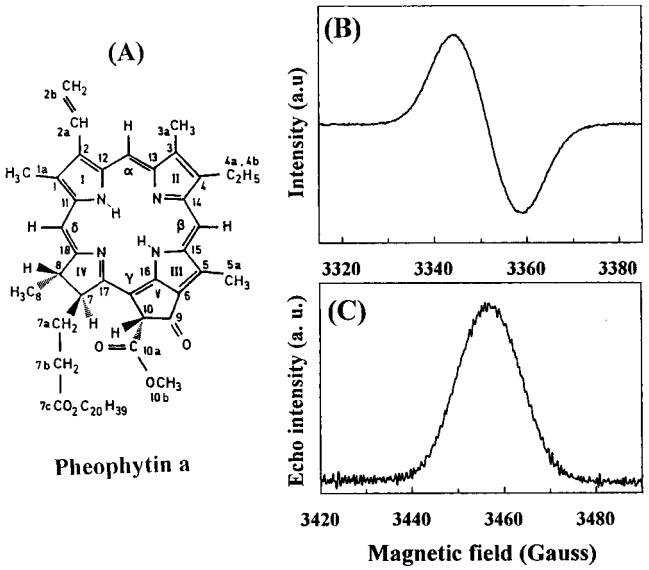

Figure 1. (A) Schematic structure of the pheophytin-α molecule. (B) X-band EPR spectrum of Pheo$^-$ in Mn-depleted [^{14}N]PSII membranes. Experimental conditions: sample temperature, 42 K; microwave frequency, 9.415 GHz; microwave power, 50 μW; modulation amplitude, 2 G; modulation frequency, 50 kHz. (C) Amplitude of the electron spin echo of Pheo$^-$ resulting from a two-pulse sequence, as a function of the magnetic field; the same sample as in (B) was used. Experimental conditions: sample temperature, 45 K; τ = 144 ns, time interval between succesive pulse sets, 5 ms; microwave frequency, 9.65 GHz.

about 350−400 ns; at longer τ values a weaker very broad component is resolved. The frequency-domain spectra for a series of τ values are depicted in Figure 2B.

The spectra are dominated by a sharp feature at 2.4−2.6 MHz with additional weaker peaks at 0.7−0.8 MHz and broad features at 3−6 MHz; in addition a complicated pattern of low-intensity peaks is observed. The intensities of the peaks vary as a function of the τ value. At long τ values only the peak at 2.4−2.6 MHz is resolved accompanied by the weaker peaks at 0.5−0.7 MHz, while at these τ values the peak at 0.2 MHz attains increased intensity; the latter corresponds to the broad feature observed at the corresponding long τ values in the time-domain spectra in Figure 2A. The broad features at 3−5 MHz are resolved only for τ values up to 280 ns. Weak peaks disposed symmetrically around the ^{1}H Larmor frequency at ∼15 MHz of weakly coupled protons are also resolved at certain τ values (not shown).

The observed frequency pattern for Pheo$^-$ in [^{14}N]PSII, in Figure 2B, is rather complicated; in principle the observed peaks arise from either ^{1}H or ^{14}N nuclei interacting with the electron of the Pheo$^-$ radical. To assign the observed peaks, we performed ESEEM for Pheo$^-$ generated in ^{15}N-labeled PSII. The corresponding field swept spectrum is displayed in the inset of Figure 3A.

[^{15}N]PSII. Representative time-domain stimulated ESEEM spectra of the Pheo$^-$ radical recorded in ^{15}N-labeled PSII are displayed in Figure 3A. A deep modulation of the echo decay with a period of ∼1.6 μs is the dominating feature of the spectra. In addition, shallower modulation harmonics with shorter periods can be resolved at certain τ values. The corresponding frequencies can be analyzed by referring to the frequency-domain spectra which are presented in Figure 3B. The sum of the Fourier transform of the ESEEM recorded at 20 τ values (from 120 to 744 ns in steps of 32 ns) is displayed at the top of Figure 3B. In the low-frequency part of Figure 3B an intense feature with a maximum at 0.65 MHz is observed; this corresponds to the ∼1.6 μs modulation period. A broader feature at about 1 MHz and weaker features in the range 1.5−2.5 MHz are resolved at certain τ values. At higher frequencies, better resolved in an expanded scale (see for example the dashed line in Figure 3B), a number of weak components are resolved. By comparison of Figures 2B and 3B it is immediately seen that the main low-frequency lines of Figure 2B are absent in Figure 3B. This allows an unequivocal assignment of these low frequencies to nitrogen modulations.

The four nitrogens of the macrocycle of the pheophytin are obvious candidates for the observed nitrogen modulations. Our approach for the analysis of the ESEEM data was to perform 2D-HYSCORE experiments[9] in order to identify the correlated peaks originating from the same nucleus.[9,10] Then, systematic numerical simulations of the observed ESEEM spectra for the Pheo$^-$ in ^{15}N-labeled PSII were carried out; the estimated ^{15}N hyperfine coupling constants were subsequently scaled by $\mathbf{g}_N(^{15}N)/\mathbf{g}_N(^{14}N) \approx 1.4$ and used in simulations for the determination of the ^{14}N quadrupole interaction parameters.

2D-HYSCORE. The HYSCORE experiment, like the 1D-stimulated ESEEM, suffers from the τ-suppression effect;[9c,d] if one of the two conjugated nuclear transitions is suppressed, then in the 2D-HYSCORE spectrum in the frequency domain the corresponding correlation peak has diminished amplitude. Therefore, we have performed several 2D-HYSCORE experiments employing six different τ intervals between the first two pulses in the four-pulse sequence. Representative contour plots of 2D-HYSCORE spectra for Pheo$^-$ in [^{15}N]PSII are displayed in Figure 4A,B for two τ values of 240 and 80 ns, respectively. Correlation lines are resolved in both quadrants. In the (+, +) quadrant in Figure 4A two sets of symmetric ridges are resolved; since they are symmetric with respect to the diagonal, we will refer to only one of the two halves. By referring to Figure 4A for τ = 240 ns, one set has lines which are perpendicular to the diagonal and have edges from (2.2 MHz, 1.4 MHz) to (1.8 MHz, 1.6 MHz); at τ = 80 ns this set of cross-peaks is suppressed. According to the theoretical correlation features in Figure 5, this pattern corresponds to a weak isotropic coupling with modest anisotropy like in Figure 5A; further analysis by computer simulations of this set of correlation features at various τ values shows that it originates from a hyperfine coupling tensor, which we term **A**, with principal values of either (1.4 MHz, 1.4 MHz, 0.5 MHz) or (0.4 MHz, 0.4 MHz, 1.1 MHz) within an error of ±0.2 MHz. The second set of features concerns the strong ridges which are well resolved for 240 ns as well as for 80 ns and which run almost parallel to the frequency axes and have comparable intensity in both quadrants. These features arise from hyperfine coupling close to the matching condition; see for example Figure 5D. In the 1D-ESEEM spectrum these features are correlated with the strong peak at 0.6 MHz observed of Figure 3B. The corresponding hyperfine coupling tensor, which we term **B**, is estimated to have principal values of (1.8 MHz, 1.8 MHz, 4.2 MHz) within an error of ±0.2 MHz.

For the case of the strong hyperfine coupling the (+, −) quadrant for τ = 80 ns in Figure 4B, is quite informative where two sets of extended ridges running parallel to the diagonal are resolved. Again by referring to the model calculations in Figure 5F, these shapes correspond to hyperfine coupling with both the isotropic and anisotropic part being large compared with the nuclear Larmor frequency. At τ = 240 ns these ridges are suppressed and are only partially resolved; See Figure 4A. The model calculations show that the characteristic low-frequency curved edge of these features is more sensitive to the hyperfine coupling constants than the part parallel to the diagonal. Further analysis of these features by computer simulation allows the resolution of two hyperfine coupling tensors; one corresponds to the correlation ridge which in Figure 4B extends from (0.8

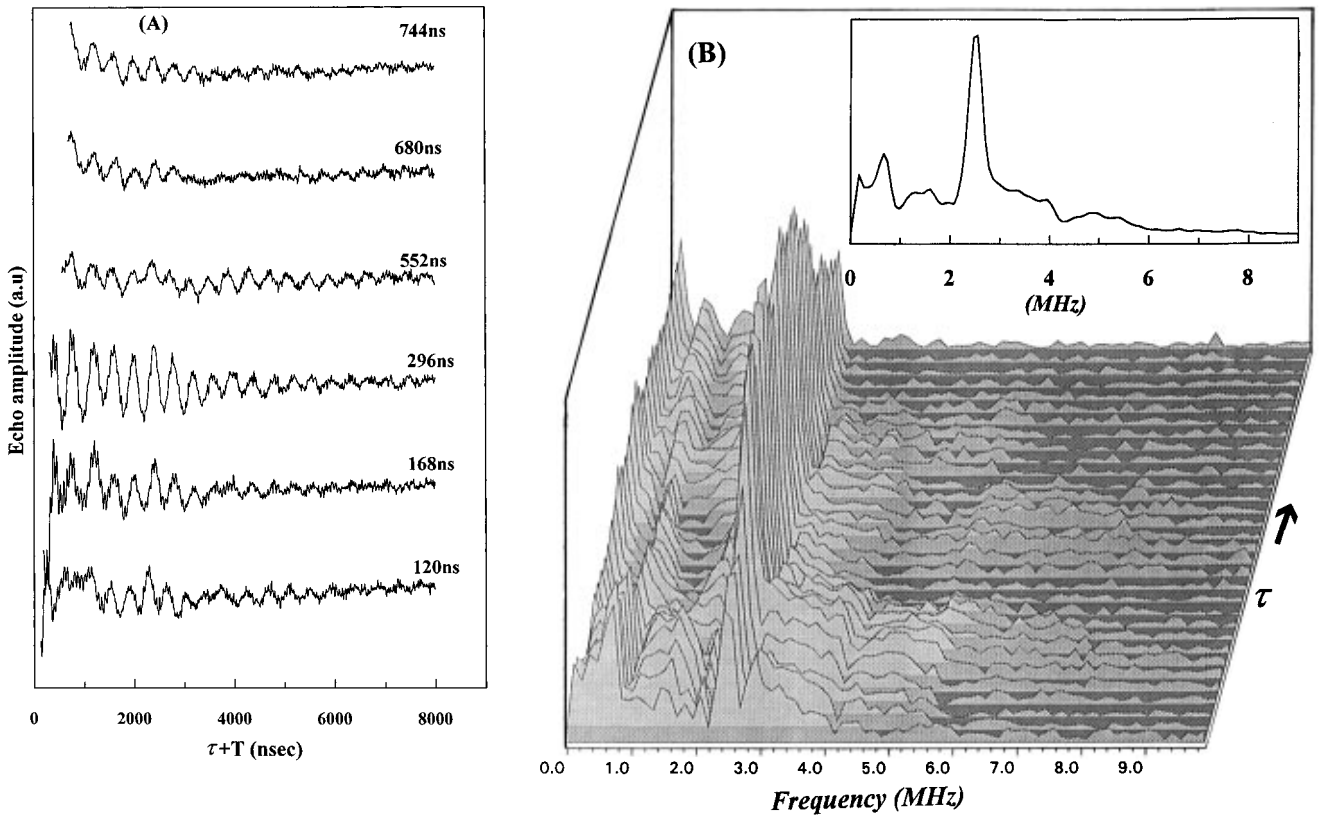

Figure 2. (A) Experimental stimulated echo ESEEM signal of Pheo⁻ in [¹⁴N]PSII recorded at the indicated τ values (period between the first and second microwave pulses). (B) Power calculation of the Fourier transform at a series of τ values from 120 to 744 ns in increments of 16 ns. Inset: sum of the Fourier transform of stimulated-echo ESEEM displayed in (B). Experimental conditions: microwave frequency, 9.66 GHz; magnetic field strength, 3453 G; sample temperature, 42 K; time interval between successive pulse sets, 5 ms; 400 events were averaged for each time point. For each τ value the initial T value (period between the second and third microwave pulses) was 16 ns, and 1024 data points were collected at 8 ns intervals; a four-step phase cycle was employed.

MHz, −2.6 MHz) to (4.6 MHz, −6.2 MHz). This tensor, which we term **C**, is estimated to have principal values of (2.1 MHz, 2.1 MHz, 18.5 MHz) within an error of ±0.4 MHz. A second set of correlation ridges is partially resolved in the (+, −) quadrant. At $\tau = 80$ ns in Figure 4A it has a low frequency edge at (1.0 MHz, −3.4 MHz), a partially resolved part running parallel to the diagonal, see for example the point (2.0 MHz, −4.1 MHz), while its high-frequency part is less well resolved. These features are not accounted for by tensor **C**. After analysis of the low-frequency part, and taking into account data recorded at other τ values and at lower contour intensities, the principal values of the corresponding tensor, which we term **D**, are estimated to be (2.9 MHz, 2.9 MHz, 30.8 MHz) within an error of ±0.8 MHz.

In summary the HYSCORE spectra for Pheo⁻ in [¹⁵N]PSII allow the resolution of four sets of hyperfine coupling constants. We point out the enhanced resolution of the HYSCORE experiment compared to the 1D-stimulated ESEEM; for example, in the case of the strong coupling tensors **C** and **D**, the corresponding peaks in the 1D-stimulated ESEEM spectra are highly dispersed and thus are barely resolved. At most they are only partially resolved in the spectra of Figure 3B (e.g., the features around 5−6 MHz).

Simulations. The 2D-HYSCORE experiment allowed the assignment of the correlated transitions for the nuclear spins and an estimation of the ¹⁵N hyperfine coupling constants; by using this information, the simulation of the 1D-ESEEM spectra allows a refinement of these parameters. Figure 6 shows simulations of the stimulated ESEEM spectra for Pheo⁻ in [¹⁵N]-PSII; the simulations were performed starting with the four hyperfine coupling tensors estimated from the HYSCORE experiment for Pheo⁻ in [¹⁵N]PSII. Initially, the tensors were assumed to be axially symmetric; subsequently a progressively increased degree of rhombicity was introduced and the quality of the simulation was judged from comparison with the experimental spectrum. In Figure 6 we display the simulated spectra for the ESEEM of Pheo⁻ in [¹⁵N]PSII; the individual contributions from the four tensors **A**, **B**, **C**, and **D** in accordance with the HYSCORE results, are shown. At the top of Figure 6 the total simulated spectrum obtained by use of the four tensors and after application of the product rule for multiple nuclear coupling[4d] is displayed. The simulations show that the experimental spectra are well described by tensors with relatively small rhombic character and that the combination lines arising from multiple nuclear coupling are too weak to be resolved; the resulting hyperfine coupling tensors after being scaled for ¹⁴N are summarized in Table 1.

According to this analysis, the strong and relatively narrow peak at ∼0.6 MHz in the ESEEM for Pheo in [¹⁵N]PSII arises from a hyperfine coupling tensor, named **B** in Table 1, with considerable anisotropy. The fact that in spite of this anisotropy this line attains strong intensity and relatively narrow line width deserves some comment; the characteristic line narrowing phenomenon in ESEEM spectroscopy has been thoroughly analyzed for $S = 1/2$, $I = 1/2$ systems[18a,b] and more recently for $S > 1/2$, $I = 1/2$ systems.[18c] For an $S = 1/2$, $I = 1/2$ system, when $|2A_{iso} + T|$ becomes comparable to $4\nu_I$, the frequency dispersion arising from the anisotropic hyperfine interactions in the low-frequency nuclear transition vanishes; this results from the compensation of dispersive terms bearing opposite algebraic signs. In the ideal case of exact matching, the frequency of the dispersion-free peak is $3|T|/4$. In the case of small anisotropy in the hyperfine interaction the ¹⁵N-ESEEM consists of a strong narrow peak close to zero frequency and a

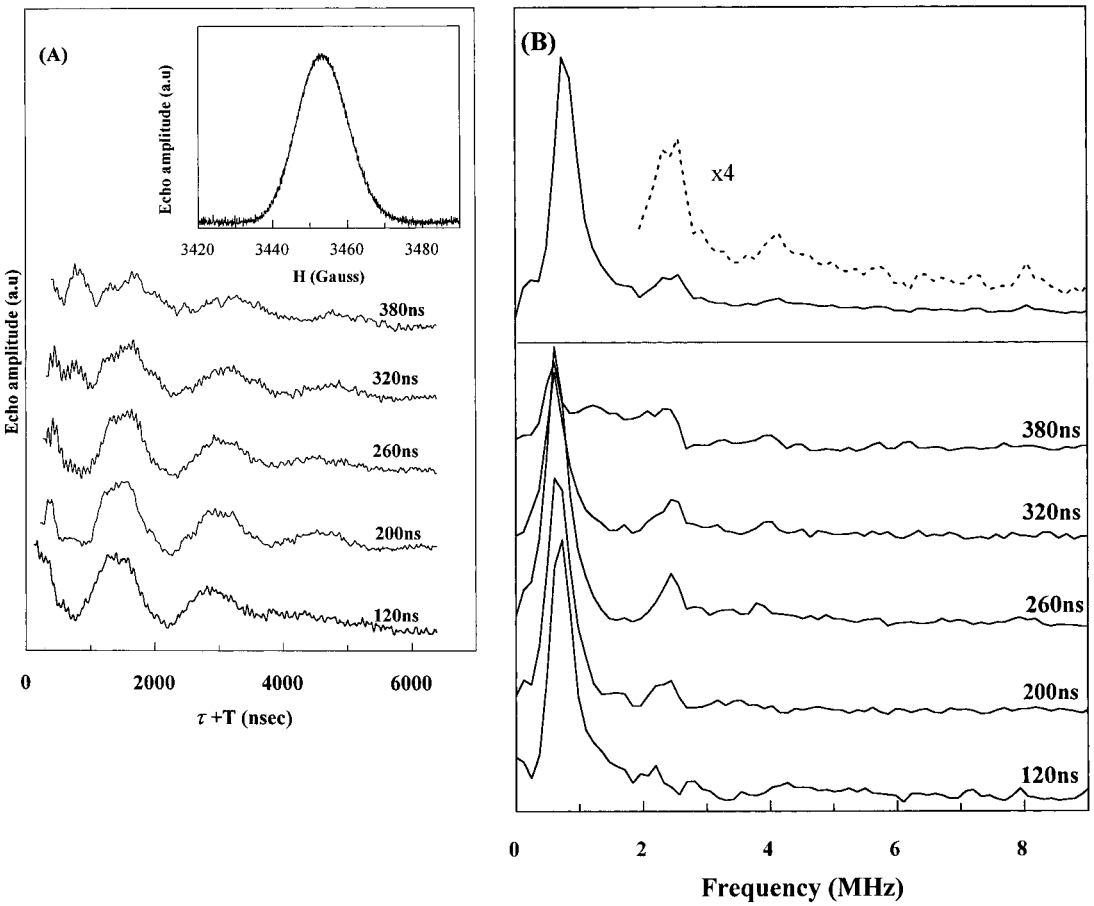

Figure 3. (A) Stimulated echo ESEEM signal of Pheo$^-$ in ^{15}N-labeled PSII recorded at the indicated τ values. Inset: Amplitude of the electron spin echo of Pheo$^-$ in [^{15}N]PSII resulting from a two-pulse sequence, as a function of the magnetic field. (B) Power calculation of the Fourier transform of the traces displayed in (A). Top: sum of the Fourier transform for 20 τ values from 120 to 760 ns in steps of 32 ns. Experimental conditions: microwave frequency, 9.65 GHz; magnetic field strength, 3455 G; other conditions as in Figure 2.

conjugated weak peak at $\sim 2\nu_I$; this has been observed experimentally in the ESEEM of the acceptor-side semiquinone Q_A^- in [^{15}N]PSII.[8h] For tensor **B** in Table 1 the rather modest deviation from the matching condition is the origin of the enhanced intensity of the peak at 0.6 MHz.

^{14}N Quadrupole Interaction Constants. Most of the ^{14}N-ESEEM spectra reported previously in the literature fall into two hyperfine coupling ranges which have been treated in model calculation studies;[19c,d] in most of the cases the anisotropic hyperfine coupling is small with respect to the isotropic term. The first, best known, ESEEM spectral type arises when $\nu_I = A_{iso}/2$ and is termed as the "exact cancellation condition".[19c] Typically the frequency domain spectra obtained under this condition consist of three sharp, low-frequency lines and a broader feature at higher frequency, typically 4−6 MHz;[20a] in the time domain the modulation is deep, on the order of half of the maximum echo amplitude detected. See for example the simulated spectrum in Figure 7B for $A_{iso} = 2.0$ MHz. Inspection of the time- and frequency-domain spectra for Pheo$^-$ in [^{14}N]-PSII in the present case shows that they do not belong to this type. In the case of deviation from the exact cancellation condition under negligible anisotropy, the modulation depth is attenuated while when $|\nu_I - A_{iso}/2| < 2K/3$, it is still possible to observe ^{14}N-ESEEM frequencies similar to those observed for exact cancellation.[19c,d]

In the second class $|\nu_I - A_{iso}/2| > 2K/3$, and when $|A_{iso}| > 2\nu_I$, typical ^{14}N-ESEEM spectra consist of just two peaks corresponding to the double-quantum nuclear transition in the two electron spin manifolds;[19c,d] see for example the simulated spectra in figure 7B for $A_{iso} > 2.5$ MHz. This type of deviation from the exact cancellation is often encountered in oxovanadium complexes;[9df,21] the same type of spectrum is expected in the case of ν_I dominating the hyperfine coupling.[22] Large hyperfine couplings have been exploited in studies of the Mn multiline signal in PSII[8c] and in T-catalase.[23]

In all the aforementioned cases the anisotropy of the hyperfine interaction is considered to be negligible. In the presence of considerable anisotropic hyperfine interaction the ESEEM spectra degrade. This is shown in Figure 7A where, for $A_{iso}/2 \approx \nu_I$, even a modest anisotropy influences drastically the peak positions and intensities. In the case when both the isotropic and the anisotropic hyperfine couplings are large, the ^{14}N-ESEEM spectra consist of only the perpendicular singularities of the powder line shapes; the remaining spectral features are so broad that they are severely damped during the instrumental deadtime.[24] This type of spectrum has been reported for the semiquinone state of copper-containing amine oxidases.[24] Usually, after scaling the ^{14}N hyperfine coupling parameters for ^{15}N, the corresponding three-pulse ESEEM spectra for ^{15}N show very small modulation depth.[24,25] Here we demonstrate that these ^{15}N modulations can be resolved due to the enhanced resolution of the HYSCORE experiment.

The hyperfine coupling constants for the ^{14}N are calculated by scaling the ^{15}N by the ratio $\mathbf{g}_N(^{15}N)/\mathbf{g}_N(^{14}N) \approx 1.4$, at the

(21) Astashkin, A. V.; Dikanov, S. A.; Tsvetkov, Y. D. *J. Struct. Chem.* **1984**, *25*, 45.
(22) Cosgrove, S. A.; Singel, D. J. *J. Phys. Chem*. **1990,** *94*, 8393.
(23) Dikanov, S. A.; Tsvetkov, Y. D.; Khahgulov, S. V.; Goldfelld, M. G. *Dokl. Akad. Nauk. SSSR* **1988,** *302*, 1255.
(24) McCracken, J.; Peisach, J.; Cote, C.; McGuirl, M. A.; Dooley, D. *J. Am. Chem. Soc*. **1992,** *114*, 3715.
(25) (a) Magliozzo, R. S.; McCracken, J.; Peisach, J. *Biochemistry* **1987**, 26, 7923. (b) Eads, C. D.; LeBrutto, R.; Kumar, A., Villaffranca, J. *Biochemistry* **1987**, *27*, 165.

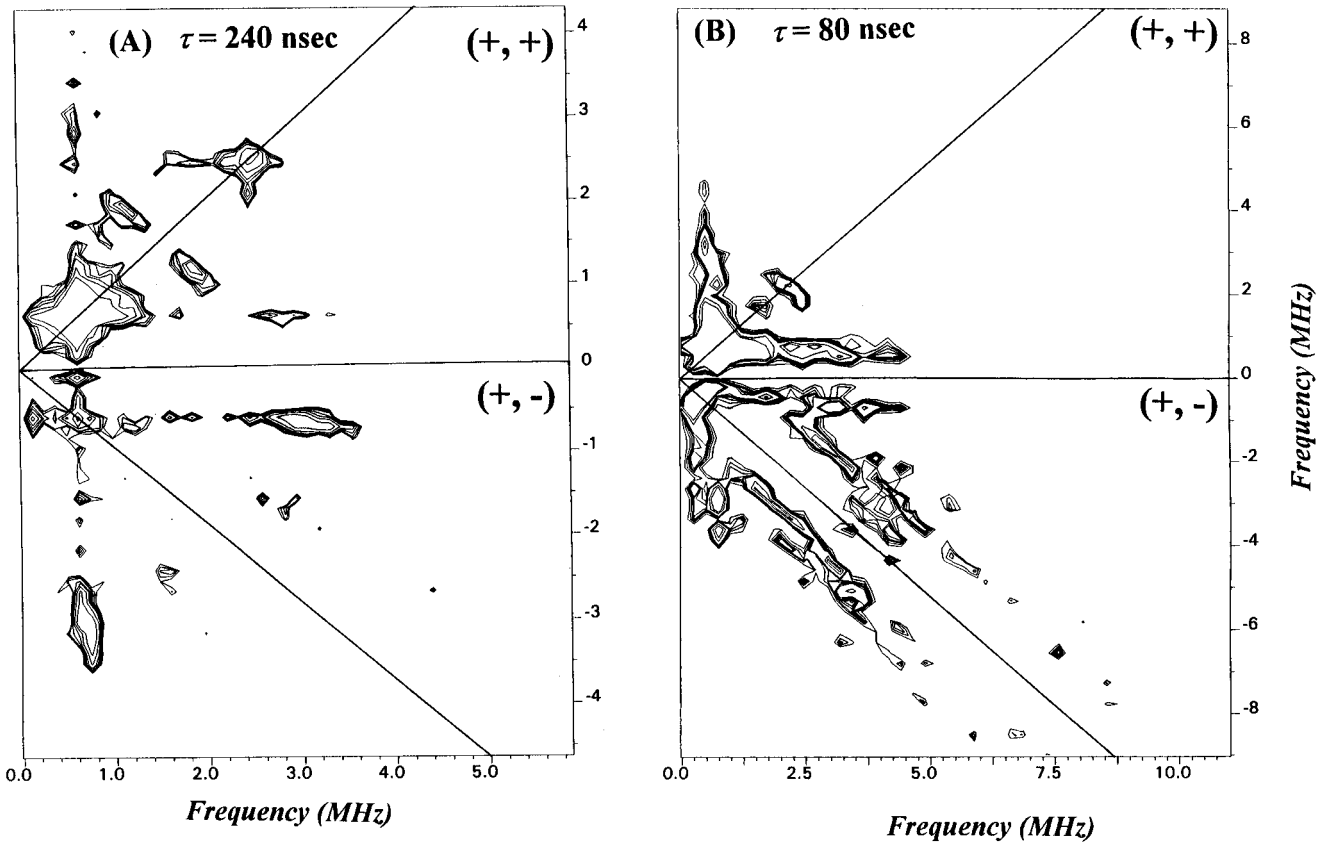

Figure 4. Experimental 2D-HYSCORE spectra (contour plots) of Pheo⁻ in [¹⁵N]PSII recorded at (a) $\tau = 240$ ns and (b) $\tau = 80$ ns. Experimental conditions: $t_1 \times t_2 = 256 \times 256$ points; start values, $t_1 = 80$ ns, $t_2 = 240$ ns; other conditions as in figure 3.

magnetic field used in these experiments. We have carried out systematic simulations of ^{14}N stimulated ESEEM spectra; our preliminary attempts to interpret the experimental spectra were directed at the simulation of the major features at 2.4−2.6 MHz and subsequently the 0.25, 0.72, and 3−5 MHz features. The requirements were primarily to reproduce the frequency positions and subsequently the basic line shapes. In the following the Euler angles were scrutinized in order to reproduce the relative intensities; representative simulated spectra showing the effect of the angle β are displayed in Figure 7C. Since it is known that the relative intensities in these experiments might be perturbed for example due to deadtime and nonideal pulses,[30] it is preferable to compare a series of τ values; in fact the τ-suppression effect was proven to be of critical importance for the selection of the possible parameters. In the case of weak hyperfine interaction, tensors **A** and **B**, the quadrupole interaction plays a dominant role in the determination of the modulation frequencies; the frequency positions are sensitive to the values of K and η while the Euler angles drastically affect the relative intensities. Thus, for the weakly coupled nitrogens the nuclear quadrupole interaction parameters are determined with a high degree of accuracy. The simulated spectra for Pheo⁻ in [^{14}N]-PSII are displayed in Figure 8. Each simulation was performed by using one of the four ^{14}N individual hyperfine coupling tensors **A**, **B**, **C**, and **D** determined from the analysis of the ^{15}N-ESEEM; the quadrupole parameters used in the simulations are listed in Table 1. At the top of Figure 8 the total simulated spectrum obtained by using the four tensors and including the product rule according to eq 5 is displayed; the calculations show that essentially no combination line is resolved. Tensor **B** reproduces the main peaks in the spectra in Figure 2B, for example, at 0.7 and 2.6 MHz, while tensor **A** results in weak features at <2 MHz. Close inspection of the relative intensity and the τ dependence of the strong peak at 2.6 MHz shows that it contains contributions from more than one transition at this frequency; as shown in Figure 8 it also contains contributions from a weaker peak resulting from tensor **C**. The part of the 2.6 MHz peak arising from tensor **B** has intensity which varies slowly as a function of τ in contrast to the fast variation of the intensity of the 2.6 MHz peak originating from tensor **C**. We find that tensor **D** with components (2.1 MHz, 2.1 MHz, 22.0 MHz) and nuclear quadrupole parameters similar to those of tensor **C** reproduces the frequency positions and the τ dependence of spectral features at 3−6 MHz as is seen in Figure 8. We find that for tensors **C** and **D** even a small deviation of the angle β from zero results in a drastic diminution of the spectral features; the angles α and γ are set arbitrarily equal to zero since they have no effect on the simulated spectra. The determined values for the hyperfine and nuclear quadrupole coupling constants are summarized in Table 1.

Discussion

Assignment of the Observed Nitrogen Couplings. In principle the observed nitrogen couplings originate from the four pyrrole nitrogens of the pheophytin macrocycle; see Figure 1A. In addition we consider the possibility that some of them may originate from nitrogen nuclei from the protein environment of Pheo⁻ interacting with the electron spin; for example, this type of interaction is detected in the case of the semiquinone anion in PSII[8g,h] and in the bacterial reaction center.[6g] In the case of photosynthetic pigments the unpaired electron spin density is expected to be highly delocalized; see for example ref 5e. The ^{14}N- and ^{15}N-ESEEM spectra of BChl and Chl cations are complex and show that the hyperfine interactions for the nitrogens are highly anisotropic.[6,7] In previous ^{14}N-ENDOR data for Pheo⁻ *in vitro* in liquid solution the detection of strong isotropic hyperfine couplings for two nitrogens was reported;[5c] the corresponding couplings, which are listed in Table 1, are in the range 5−7 MHz. In addition the existence of two weak nitrogen hyperfine couplings were postulated, although they

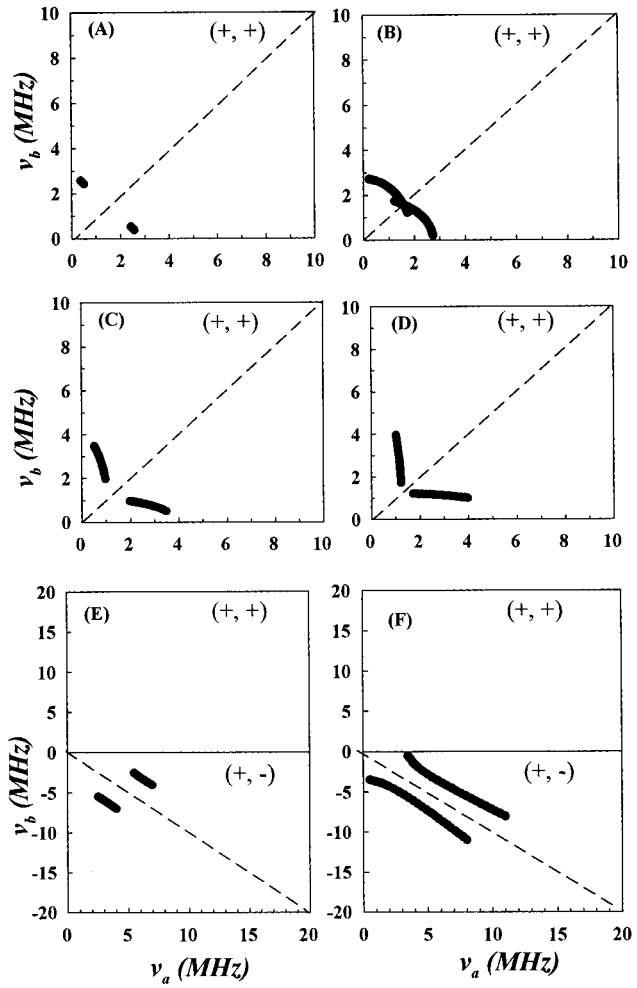

Figure 5. Theoretical line shapes of the cross-peaks for 2D-HYSCORE spectra calculated by use of eq 4 for $\nu_I = 1.495$ MHz. The intensity of the lines in the (+, +) or in the (+, −) quadrant is determined according to the amplitude factors given in eq 8; in each panel only the quadrant with the stronger lines is displayed. The isotropic, A_{iso}, and the anisotropic, T, hyperfine coupling parameters used are (A_{iso}, T) = (0.4 MHz, 0.2 MHz) in panel A, (1.0 MHz, 0.8 MHz) in B, (1.7 MHz, 0.8 MHz) in C, (2.4 MHz, 1.1 MHz) in D, (4.0 MHz, 0.2 MHz) in E, and (6.0 MHz, 4.0 MHz) in F.

were not resolved by ENDOR. On the basis of ^{14}N- and ^{1}H-ENDOR data, molecular orbital calculations indicate that the non-protonated nitrogens of Pheo$^-$ *in vitro* (see Figure 1A) bear considerable spin density while the spin density on the protonated nitrogens is expected be negligible.[5d,37b] An analogous trend is observed in the free-base porphine.[26] ^{1}H-ENDOR data for Pheo$^-$ in PSII in thylakoid membranes[5b,d] and D_1D_2cyt b_{559} particles[5d] indicate that the spin density distribution in Pheo$^-$ in the reaction centers is comparable, although not identical, to that for the Pheo$^-$ radical *in vitro.* According to this analysis we consider that tensors **A** and **B** in Table 1 correspond to the two protonated nitrogens of Pheo$^-$ and tensors **C** and **D** to the nonprotonated nitrogens; see Figure 1A. No couplings between the Pheo$^-$ radical and protein nitrogens, like those seen for other radicals,[8g,h,6h] were resolved.

Spin Densities. For a nitrogen nucleus with adjacent, equivalent carbons, the observed isotropic hyperfine couplings may be analyzed with a relation of the form $A_{iso} = Q_{NX}{}^{N}\rho_{NX} + 2Q_{CN}{}^{N}\rho_{C}$, in which the X serves to distinguish the presence of a either a nonbonding electron lone pair (X = P) or a bound proton (X = H).[26,27e] Despite numerous EPR studies of nitrogen-containing π-radicals in solution,[27] no definitive evaluation of the constants $Q_{NX}{}^{N}$ and $Q_{CN}{}^{N}$ has been established. A wide spread of values in the range 53−87 MHz for $Q_{NP}{}^{N}$ and −11 to +26 MHz for $Q_{CN}{}^{N}$ has been reported, while $Q_{NH}{}^{N}$ has been reported to be about 25% greater than $Q_{NP}{}^{N}$.[27] Single-crystal ESEEM data show that, in the free-base porphin, to a good approximation a simple relation between the anisotropic hyperfine interaction (T) and the nitrogen spin densities (ρ_N) is $T \approx 53\rho_N$ MHz.[26] In the same system, the isotropic part of the interaction is found to be strongly influenced by multinuclear interactions[26] and values of $Q_{NP}{}^{N} = 54$ MHz, $Q_{NH}{}^{N} = 70$ MHz, and $Q_{CN}{}^{C} = -7$ MHz were estimated. We consider the the porphin molecule is a better model for the Pheo macrocycle than for example the aliphatic nitrogens.[27] Using the Q values estimated for the porphine molecule and the spin densities estimated by molecular orbital calculations for a model Pheo$^-$ radical,[5d] we calculate the hyperfine coupling constants which are listed in Table 1. It is seen that the unprotonated nitrogens are expected to have A_{iso} and T much larger than the ^{14}N nuclear Larmor frequency while the protonated nitrogens are expected to have small A_{iso} and T; this is in agreement with the assignment of the hyperfine tensors for Pheo$^-$ in PSII that we make in Table 1. The differences observed between the nitrogen hyperfine couplings observed for Pheo$^-$ in PSII and the calculated values listed in Table 1 are modest.

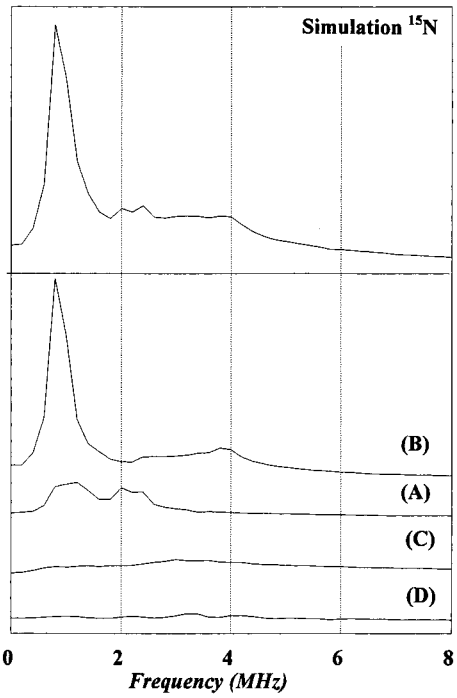

Figure 6. Fourier transform of theoretical simulations of three-pulse ^{15}N-ESEEM spectra obtained with the hyperfine coupling tensors **A**, **B**, **C**, and **D** corresponding to those listed in Table 1 after being scaled by $\mathbf{g}_N(^{15}N)/\mathbf{g}_N(^{14}N)$. Top: simulated spectrum obtained by the use the four tensors, including the product rule. Each spectrum is the sum of 20 spectra calculated for τ values from 120 to 740 ns in steps of 32 ns. Simulation parameters: microwave frequency, 9.65 MHz; magnetic field strength, 3455 MHz.

(26) Singel, D. J.; van der Poel, W. A. J. A.; Schmidt, J.; van der Waals, J. H.; de Beer, R. *J. Chem. Phys*. **1984**, *81*, 5453.

(27) (a) Ward, R. L. *J. Am. Chem. Soc*. **1961**, *83*, 3626; **1962,** *84*, 332. (b) Barton, B. L.; Fraenkel, G. K. *J. Chem. Phys*. **1964**, *41*, 1455. (c) Henning, J. C. M. *J. Chem. Phys.* **1966**, *44*, 2139. (d) Adam, J. Q.; Nisckic, S. W.; Thomas, J. R. *J. Chem. Phys.* **1966,***45*, 654. (e) Stone, E. W.; Maki, A. H *J. Chem. Phys.* **1963**, 39, 1635. (f) Atherton, N. M.; Gerson, F.; Morell, J. N. *Mol. Phys.* **1962**, *5*, 509. (g) Talcott, C. L.; Myers, R. J. *J. Chem. Phys*. **1967,** *12*, 549. (h) Carrington, A.; dos Santos-Veiga, J. *Mol. Phys*. **1962**, *5*, 21. (i) Bolton, J. R.; Carrington, A.; dos Santos-Veiga, J. *Mol. Phys*. **1962**, *5*, 456.

Table 1. Experimental and Theoretical ^{14}N Hyperfine and Quadrupole Coupling Constants for Pheo⁻ in PSII and Model Compounds[20d]

	param	**A** (N_{III})[d]	**B** (N_I)[d]	**C** (N_{IV})[d]	**D** (N_{II})[d]	ref
14N-ENDOR	$\|A_{iso}\|$	<2	<2	5.16	6.42	5c
theoretical[a,b]	$\|A_{iso}\|$	0.8	1.4	6.2	9.4	
	$\|T\|$	0.8	0.9	5.7	8.7	
ESEEM of Pheo⁻ in PSII[c]	A_{xx} (MHz ± 0.05)	0.9	1.4	1.4	2.1	this work
	A_{yy} (MHz ± 0.05)	1.0	1.0	1.4	2.1	this work
	A_{zz} (MHz ± 0.05)	0.5	2.7	12.7	22.0	this work
	A_{iso} (MHz ± 0.05)	0.8	1.7	5.2	8.7	this work
	α, β, γ (deg ± 10)	30, 90, 20	20, 10, 0	0, 0, 0	0, 0, 0	this work
	e^2qQ/h (MHz ± 0.05)	2.55	2.85	3.20	3.10	this work
	η ± 0.05	0.40	0.30	0.10	0.10	this work

[a] Molecular geometry of the Pheo⁻ molecule as in Figure 1A. [b] Calculated from p_z spin densities, at carbon ρ^{π}_C and nitrogen positions ρ^{π}_N by use of the equations $A_{iso} = Q_N^N \rho^{\pi}_N - 14\Sigma\rho^{\pi}_C$ and $T = 53\rho^{\pi}_N$ with $Q_N^N = 54$ and 70 MHz for the pyrrole and N−H nitrogens, respectively. The unpaired spin densities on the nitrogens ρ^{π}_C and the one-bond neighboring carbons ρ^{π}_C are taken from ref 5d. [c] The errors in parentheses refer to tensors **A** and **B**; for tensors **C** and **D** the errors are A_{ii} ± 0. 4 MHz, e^2qQ/h ± 0.1 MHz, and η ± 0.1 MHz. [d] Tensor (assignment).

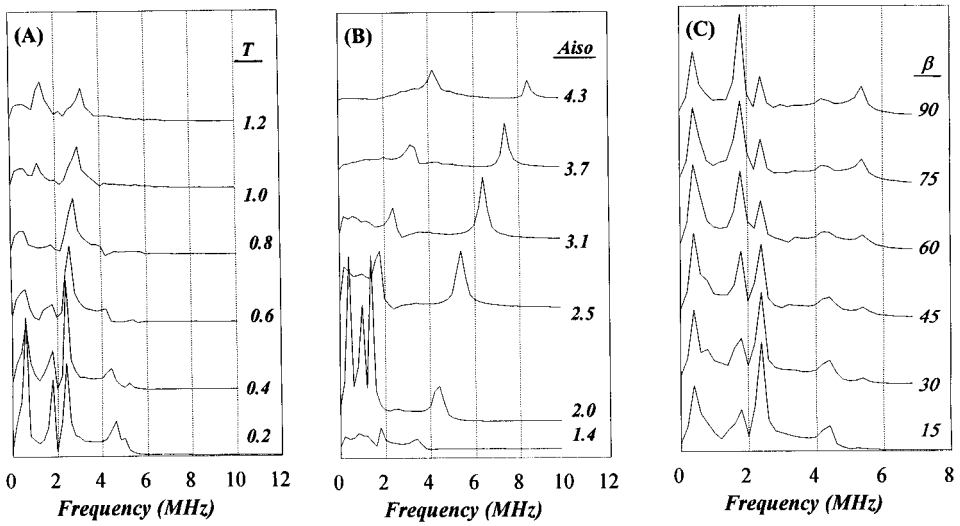

Figure 7. Fourier transform of theoretical simulations of three-pulse ESEEM spectra for a single ^{14}N nucleus. (A) Effect of the anisotropic hyperfine coupling; the value of T is varied from 0.2 to 1.2 MHz. Other simulation parameters are $A_{iso} = 2.0$ MHz, $e^2qQ = 2.65$ MHz, and $\eta = 0.3$. (B) Effect of A_{iso} ranging from 1.4 to 4.3 MHz with $T = 0.13$ MHz, $e^2qQ = 1.5$ MHz, and $\eta = 0.5$. (C) Effect of the angle β ranging from 15° to 90° with A_{iso}=1.97 MHz, $e^2qQ = 2.65$ MHz, $\eta = 0.3$, $T = 0.35$ MHz, and $(\alpha, \gamma) = (0°, 0°)$. Common simulation parameters in all panels: τ =180 ns, microwave frequency, 9.65 MHz; magnetic field strength, 3453 MHz.

It is anticipated that the solvating environments for Pheo⁻ in the reaction center of PSII and the model radical in frozen solution differ. The present ESEEM data indicate that despite these differences the unpaired spin densities on Pheo⁻ in PSII and in frozen solutions are comparable. Overall this suggests that the dielectric properties of the medium exert little influence on the distribution of the unpaired spin density and hence the energy of the singly occupied molecular orbital of the pheophytin radical.[20e] However, it is possible that *local* interactions with the protein environment, like hydrogen bonding,[33] may modify the spin density distribution in Pheo⁻ in the PSII reaction center.

We recently showed that the non-heme iron of PSII enhances the spin−lattice relaxation of the pheophytin radical.[3] The possibility of the modification of the spin density of Pheo⁻ due to the magnetic interaction with the iron was examined by comparing the ESEEM of Pheo⁻ in PSII membranes with the non-heme iron in the high-spin ($S = 2$) or in the low-spin diamagnetic ($S = 0$) state after treatment with CN.[34] The ESEEM of Pheo⁻ in the CN-treated [^{14}N]PSII (data not shown) was found to be indistinguishable from that for Pheo⁻ shown in Figure 2. Thus the interaction with the iron does not measurably modify the spin density of the unpaired electron on the pheophytin.

Quadrupole Interactions. For the protonated nitrogens in Pheo⁻, the observed coupling constants listed in Table 1 are comparable to that for the protonated nitrogens of the free-base porphine[26] (2.24 MHz), and both are larger than the value of 2.06 MHz obtained by nuclear quadrupole resonance for crystalline pyrrole.[28] For the unprotonated nitrogens a reduction of $|e^2qQ/h|$ is observed in Pheo⁻ (3.1−3.2 MHz) as compared to that found for azines studied in non-hydrogen-bonding solids and in the gas phase (4.2 MHz)[32] but is similar to the value reported for the unprotonated nitrogens in the free-base porphine[26] (3.32 MHz). According to the Townes and Daily model,[29] the decrease in the nuclear quadrupole coupling constant indicates that the nitrogen has lost some of its lone-pair character (*vide infra*). Also a polarization of the electrons in the neighborhood of the ^{14}N nucleus is expected to affect mainly the quadrupole coupling constant and, less, the electric field gradient.[31] The polarization may be due to hydrogen-bonding or to electrostatic effects.[26]

The relative σ- to π-spin density determines the orientation of the principal nuclear quadrupole interaction axes. In pyrrole, the molecular symmetry ensures that one field-gradient axis is perpendicular to the molecular plane,[31] that another axis lies along the NH bond, and that the third, lying in the molecular plane, is perpendicular to these two. If the N−C σ-spin−orbital populations are less than the N−H σ-orbital populations, then the x axis will lie along the N−H bond[31] which was also found to be the case for the protonated nitrogens in the free-base porphine;[26] furthermore, in the same system the z axis was found to be perpendicular to the molecular plane. On the basis of the similarities between the hyperfine and quadrupole coupling constants for the free-base porphine and Pheo⁻ in PSII, it is

(28) Schempp, E.; Bray, P. J. *J. Chem. Phys.* **1968**, *48*, 2380.

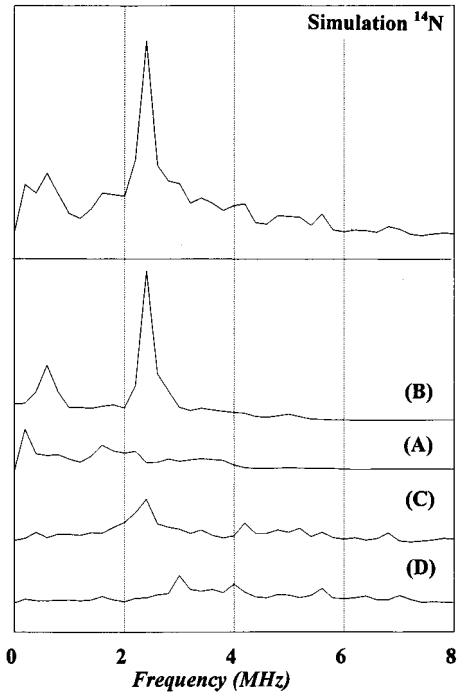

Figure 8. Fourier transform of theoretical simulations of three-pulse ^{14}N-ESEEM spectra obtained with the hyperfine and quadrupole coupling tensors **A**, **B**, **C**, and **D** corresponding to those listed in Table 1. Top: simulated spectrum obtained for the four tensors including the product rule. Each spectrum is the sum of 20 spectra calculated for τ values from 120 to 740 ns in steps of 32 ns. Simulation parameters: microwave frequency, 9.65 MHz; magnetic field strength, 3453 MHz.

tempting to extrapolate this picture in the case of Pheo$^-$. The validity of this assignment has to be tested for example by ESEEM studies on single crystals of Pheo$^-$.

In the case of Pheo$^-$ in PSII the observed small deviations from axial symmetry for the hyperfine tensors of the protonated nitrogens might reflect a nonaxiality of the molecular axis system. In the case of the nonprotonated nitrogens the large value of A_{zz} and its large difference from A_{xx} and A_{yy} values leads to the z axis being little influenced by factors other than local structure, specifically the orientation of the nitrogen p-π-orbital.[26] Analogous observations based on ESEEM data for the free-base porphine in single crystals have been interpreted as suggesting a tilt of the pyrrole rings containing the unprotonated nitrogens above and below the mean molecular frame;[26] this tilt has been observed in single crystals of free-base porphine.[35] Interestingly, it was reported that in the case of the triplet state of the free-base porphine an intramolecular hydrogen bonding leads to an increased polarization of the NH bond and consequent permutation of the x and y axes.[26] In principle it is possible that the observed deviation between the z axes of the hyperfine and the quadrupole tensor of the protonated nitrogen of Pheo$^-$ in PSII may arise from a hydrogen-bonding effect in the reaction center of PSII. However, it is considered that structural distortions may cause analogous effects; such a distortion might be a "puckered" ring of the type observed in the single crystals of the pheophorbide.[37] A rotation of the vinyl group at position 2 relative to the molecular plane of Pheo$^-$ is another type of possible structural distortion; molecular orbital calculations show that a change of the orientation of the vinyl group may induce a modification of the spin density on Pheo$^-$.[5d,37b] We notice that the spin densities used for the calculation in Table 1 were performed for the case were the 2-vinyl group of Pheo is rotated by 14° out of the molecular plane.[5c]

In nonadiabatic electron transfer the rates of long-range electron transfer depend critically on the distance-dependent overlap of the donor/acceptor electronic wave functions;[36] any mechanism resulting in a spread of the electron cloud is expected to influence the electron transfer rate. The present ESEEM data together with the ^{1}H-ENDOR data[5d] provide a complete picture of a highly delocalized distribution of the unpaired spin density on pheophytin in PSII, which is relevant to its role in the electron transfer in the reaction center. It has been postulated that the orientation of the 2-vinyl group relative to the molecular plane could affect the optimization of the donor/acceptor orbital overlap and thereby the electron transfer[5d,37b] in the reaction center of PSII. The present study demonstrates that the ESEEM data contribute useful information relevant to a deeper understanding of the relation between the structure and the electron transport function in photosynthetic reaction centers.

Conclusions

By the use of the ESEEM technique, we have obtained the hyperfine and quadrupole interaction constants for the nitrogens of the pheophytin anion radical in PSII. It is concluded that the weak and the strong couplings correspond to the protonated and the nonprotonated nitrogens of the Pheo$^-$ radical, respectively. In the present case the HYSCORE experiment allows the detection of strong hyperfine couplings which are generally considered to be better resolvable by ENDOR rather than ESEEM. The simulation of the 1D-stimulated ESEEM and the required consistency between the ^{15}N- and ^{14}N-ESEEM data allow a high degree of confidence in the determined hyperfine and quadrupole coupling constants listed in Table 1. This is the first ESEEM study of a pheophytin radical which is related to future studies in other photosynthetic reaction centers. The structural implications of the parameters extracted in the present work can be advanced after for example ESEEM studies of the Pheo$^-$ radical in single crystals.

Acknowledgment. We thank J. McCracken (Michigan State University) for providing us with subroutines for the simulation of the $S = 1/2$, $I = 1$ spectra. Y.D. was supported by the European Union Human Capital & Mobility Grant, Contract ERB0049GI1901. This work was also supported by the HCM Network "MASIMO", Contract ERBCHRXCT920072.

JA963293Y

(29) Townes, C. H.; Dailey, B. P. *J. Chem. Phys.* **1949,** *17*, 782.
(30) Kevan, L. In *Modern Pulsed and Continuous -Wave Electron Spin Resonance*; Kevan, L., Bowman, M. K., Eds.; Wiley: New York, 1990; Chapter 5.
(31) Lucken, W. A. C. *Nuclear Quadrupole Coupling Constants*; Academic: London, 1969.
(32) (a) Guibé, E. A. C.; Lucken. *Mol. Phys.* **1968**, *14*, 79. (b) von Borczyckoski, C.; Plato, M.; Dinse, K. P.; Mobius, K. *Chem. Phys.* **1978**, *35*, 155.
(33) Lubitz, W.; Müh, F.; Rautter, J.; Lentzian, F.; Allen, J. P.; Williams, J. C. In *Photosynthesis: from Light to Biosphere*; Mathis, P., Ed.; Kluwer Academic Publishers: Netherlands,1995; Vol. I, pp 413.
(34) Sanakis, Y.; Petrouleas, V.; Diner, B. A. *Biochemistry* **1994**, *33*, 9922.
(35) Chen, B. M. L.; Tulinsky, Jr. *J. Am. Chem. Soc*. **1972**, *94*, 4144.
(36) Marcus, R. A.; Shutin, N. *Biochim. Biophys. Acta* **1985**, *811*, 265.
(37) (a) Barkigia, K. M.; Chantranupong, L.; Smith, K. M.; Fajer, J. *J. Am. Chem. Soc*. **1988**, *110*, 7566. (b) Forman, A.; Davis, M. S.; Fujita, I.; Hanson, L. K.; Smith, K. M.; Fajer, J. *Isr. J. Chem.* **1981**, *21*, 265.